Effects of Pixel Size on Apparent Emissivity Signatures of Materials with Long-wave Infrared Spectral Characteristics

Timothy Grabowski
The Aerospace Corporation, Chantilly,VA
MS Project Paper
Rochester Institute of Technology
Center for Imaging Science
May 23, 2006

Abstract
This paper describes an airborne hyperspectral field collection campaign to spectrally image a number of uniform targets that exhibit strong reflective and/or emissive signatures within the visible to long wave infrared regions. To provide reference spectra, a representative sample from each target was obtained in order to complete full laboratory reflective/emissive profile. The uniform targets ranged from painted metal plates, to playa coated with chemicals, to everyday plastic tarps. All targets were selected because of their spectral characteristics within the .4 to 14 micron range (VNIR/SWIR/MWIR/LWIR). The Full Spectrum Collect was designed so that two airborne hyperspectral sensors could coordinate sufficiently enough to provide near simultaneous passes over each target area. The two airborne sensors tasked for this collection were SEBASS and the SpectIR instrument. In addition, one requirement of the collect called for each sensor to be flown at multiple altitudes concurrently to yield a range of pixel sizes over the same uniform targets. This paper will deal with how pixel size affects a target's apparent emissivity features in the LWIR.

1.0 Introduction

Many papers have been written on how hyperspectral imagery has been utilized to make geologic mineral classification maps[1, 2]. Other papers have delved into how varying spatial resolution at the sensor affect the accuracy of these geologic classification maps[3, 4]. This paper will discuss how varying spatial resolution will affect an individual target pixel's apparent emissivity spectrum. Previous papers have simulated larger ground sample distances (GSD) by using an averaging window to degrade the spatial domain of high-resolution hyperspectral data to much lower resolution datasets[3]. For the purpose of this paper, pixel size will be adjusted not by degraded high spatial resolution data, but by flying the sensors, which have a fixed field of view (FOV), at different altitudes above ground level (AGL).

Desired Altitude Ranges

SEBASS		
Altitude AGL (ft)	Coverage(m)	GSD (m)
1000	48	0.3749
2000	96	0.7498
3000	144	1.1246
4000	192	1.4995
5000	240	1.8744
6000	288	2.2493
7000	336	2.6242
8000	384	2.9990
9000	432	3.3739
10000	480	3.7488

Actual Altitudes Flown 3000, 4500, 6000 ft AGL

Fig. 1: SEBASS GSD/coverage with respect to altitude

From the law of conservation of energy, the conclusion can be drawn that the observed target apparent emissivity spectra over multiple altitudes, once atmospherically corrected for transmission and additive radiance, should yield the same observed radiance values, spectral band depths and features given that the pixel is 100% filled by the target. The targets for this collect were chosen for their strong spectral features (i.e. sharp emissive peaks) over the spectral range of the two airborne instruments. This will provide an opportunity to study high-resolution datasets of the same uniform targets viewed at differing altitudes. For the purposes of this paper, three man-made targets with strong spectral features within the Long-wave infrared (LWIR) region were selected for analysis. Polyester is a material that has features in both the mid and long wave regions so this was selected as one of the targets. Tyvek™ is a brand of tarp, which also possesses strong features in both regions. This was selected as the second target of interest. Styrofoam has strong features in the long-wave region and thus completes the set of LWIR data. However, Styrofoam also has strong reflective features in the lower end of the LWIR spectrum, as illustrated by its ability to reflect downwelling radiance towards the sensor.

LWIR data was selected to be the topic for this paper because of two reasons: 1) it was highly unlikely that SpectIR would be able to deliver any calibrated Visible/Near Infrared and Short-wave infrared (VNIR/SWIR) data in time to be processed, analyzed and

reported, 2) the atmospheric correction and subsequent apparent emissivity conversion routines written by The Aerospace Corporation's SEBASS team, is setup to easily process long wave infrared data. However, when processing Mid-wave infrared (MWIR) datasets, the assumptions made when dealing with (essentially ignoring) solar reflectance in the LWIR region cannot be safely made in the MWIR, so the correction/conversion routines must be tweaked.

2.0 Airborne Sensors

2.1 SpectIR

SpectIR is a small company, which owns and operates three commercial off the shelf systems hyperspectral sensors. As a deliverable, SpectIR can provide various calibrated and georeferenced data products depending on mission requirements. For this collect, two out of the three were tasked. The first was a VNIR sensor operating in the range from 10000 cm^{-1} to 22222 cm^{-1}, and a spectral resolution of 2.3 – 10nm is user adjustable. This instrument has a spatial swath of 960 pixels and three focal length options. Second, the SWIR sensor operates in the spectral range of 4080 – 10300 cm-1, and has a spectral resolution of 8.5nm. This sensor has a spatial swath of 315 pixels and three focal length options. The focal length selected for this test was set to yield 2 meter GSD everywhere with the exception of the "emplaced target" lines on the desert playa. These uniform targets were imaged at both 1 m and 2 m GSD. Between the two sensors, 227 bands were acquired over the wavelength region from 0.45-2.45 microns, having 8-12 nm bandwidths. The IFOV is one milliradian, so swath widths were 1800 meters for the 2m GSD and 900 for the 1m GSD, which was determined by the port size in the Cessna 206 used for data collection.

2.2 SEBASS

SEBASS possesses an optical bench cooled to a temperature of 10 K by use of a liquid helium and liquid nitrogen filled vacuum sealed Dewar. This is necessary in that at the center of the design are two 128 x 128 pixel "Blocked Impurity Band" focal plane arrays designed by Rockwell International, which are low noise and high quantum efficiency. The two arrays measure the two terrestrial windows in the mid and long wave region. The two focal plane arrays on the optical bench sense irradiant energy over the long wave infrared region of the spectrum (740-1320 cm^{-1}) and the mid wave infrared region (1876-4132 cm^{-1}). Each array is 128 x 128 pixels, oriented in a fashion that one axis is spatial and the other axis spectral. When operated in pushbroom configuration, data is recorded over 128 spatial pixels and 256 spectral channels. The spectral resolution is given at 7 cm^{-1} at 890 cm^{-1} and a one-milliradian field of view (~1m Ground Sample Distance (GSD) at 3000ft AGL)[5]. SEBASS can also be outfitted with custom optics to function as a lab scanner, but for most of the sensor's life, it has been flown on a Twin Otter aircraft.

Fig. 2 and 3: Illustration of SEBASS mounted inside a Twin Otter aircraft. The sensor is mounted on a roll stabilized cradle to account for tangent distortion.

The original data acquisition system of SEBASS was built around a VME bus system controlled by a Sun Sparc-20 CPU. Clock signals control the operation of the focal plane multiplexers and analog to digital converters. The microsequencer was a programmable unit capable of being adjusted in 67 nanosecond increments. 14-bit analog to digital converters converted the analog data from the two arrays to digital data that was in turn passed to a co-adder board, which integrated the data according to the signal and reset values. The co-adder board is a crucial component in the system because it allows the detector to remain extremely sensitive. Data was then sent from the co-adder to a cache RAM that had 384Mbytes. This allowed SEBASS to collect 6144 frames, or lines of data. Disk space was limited to a 10Gbyte hard drive.

Recently the data acquisition components of SEBASS were upgraded completely. All of the A-D converters have been replaced; the CPU is now a dual Xenon processor, 64-bit Windows platform with 8Gbyte of RAM and 300Gbyte amount of storage space. Where once flight collects were limited by the amount of disk storage space for hyperspectral cubes rather than aircraft fuel capacity, now the exact opposite is true. Initial rough estimates put the noise equivalent spectral radiance (NESR) curve of the mid-wave array well lower than the NESR of the old configuration. The long-wave array's NESR is minutely higher than the old configuration but with the addition of new configurable control variables (FPA gain and offsets) within the software, the current long-wave NESR curve should be able to be reduced to well below the old NESR values.

2.3 Lab Instrumentation

Lab spectra were measured using the Designs and Prototypes Model 102 portable FTIR. It is a Michelson interferometer using an Indium Antimonide (InSb) over a Mercury Cadmium Telluride (MgCdTe) detector. It has a spectral range of approximately 2-16 microns and a spectral resolution of 2 cm^{-1}. The Styrofoam test target was measured using this instrument in a controlled laboratory environment over the full spectral range of the D&P. Radiance data was recorded of the target Styrofoam and then of a blackbody set at two temperatures, ambient and again at approximately 50 degrees C. The material's apparent emissivity can then be approximated by the equation:

$$Emis = 1 - \frac{L_{tgt} - L_{BB\_cold}}{L_{BB\_hot} - L_{BB\_cold}} \qquad (1)$$

The Tyvek and polyester were measured over the 2-25 micron range using a Nicolet Magna 550 Fourier transform infrared spectrometer (equipped with a KBr beamsplitter, and a DTGS detector) using a Harrick Scientific "praying mantis" style diffuse reflectance accessory. Labsphere infragold is used for the background measurement. The spot size is 1-2mm and the resulting spectra are qualitative not quantitative, meaning spectral shape is correct but intensity is not. Each target had a relatively flat surface.

3.0 Collect

The entire Full Spectrum Collect, spanned two aircraft, four days, three states, seven sites and over one hundred and fifty flight lines. Most of the sites consisted of geologic locations of interest, some of which are privately owned. For this reason the data over these private sites is considered proprietary and will not be discussed at this time. This paper will only deal with the uniform targets located on the desert playa on Days 3 and 4 of the Full Spectrum Collect. During these two days, approximately thirty-five targets were laid on the playa and two flight lines were plotted roughly perpendicular to each other in order to achieve full coverage of all the targets at each altitude. The second day at the desert site was when all of the multiple altitude flight lines occurred, so only datasets from this day will be analyzed for the topic of this paper.

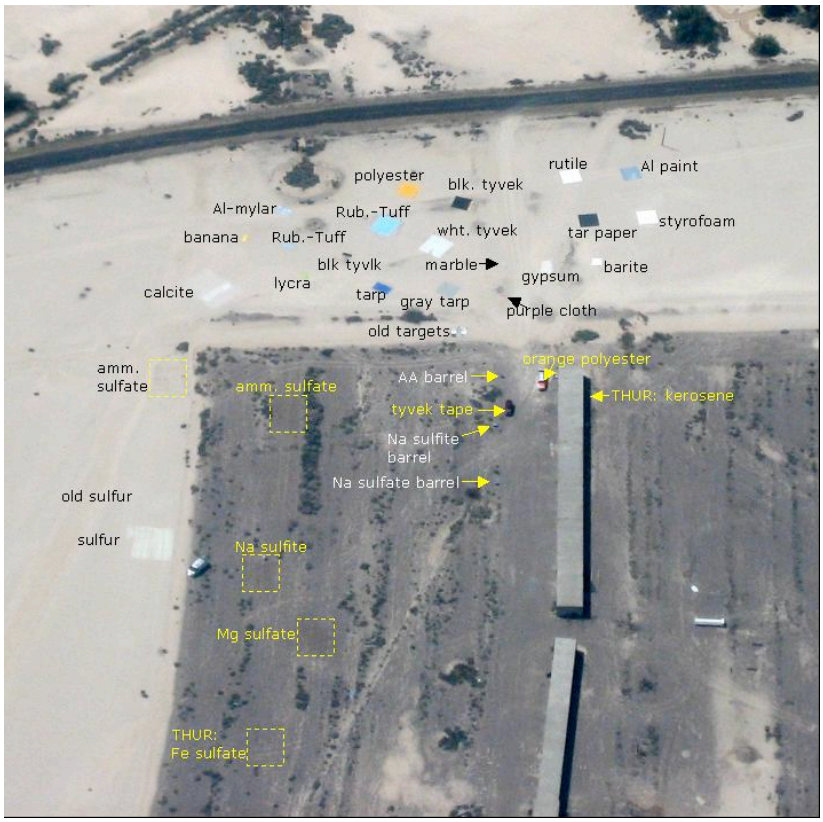

Fig. 4: Target layout.

Time (Local)	Session	Target	Altitude (ft AGL)
1140	153839	Hotel2	6000
1146	154442	Hotel1	6000
1153	155041	Hotel1	6000
1200	155829	Hotel1	4500
1207	160440	Hotel2	4500
1215	161238	Hotel2	3000
1221	161921	Hotel1	3000

Fig. 5: Log sheet for SEBASS flightlines on 5/4/06

Flight altitude restrictions were in place prior to the test, and real-time authorization of any altitude deviations from the flight plan of 7000 ft AGL was required. Due to the busy schedule of the airspace, it was originally thought that the multiple altitude flightlines would not be feasible to complete. However, both days, air traffic controllers were extremely accommodating each time the SEBASS collect team wished to adjust their altitude. As a result, multiple passes of each flight line were performed at 3000, 4500, and 6000 ft AGL. This yielded square pixels approximately 1 x 1m, 1.5 x 1.5m, and 2 x 2m respectively. Since the uniform targets chosen for analysis were 5 x 5m square, it can safely be assumed that there is at least one full pixel of target for each line and altitude. Weather each day was mild, sunny and clear.

4.0 Processing

Once a hyperspectral image cube has been acquired, the raw file contains simple digital counts, in the case of SEBASS, the 14-bit analog to digital converters will give values within the range of 0-16383.

1) Run the raw .dat files with The Aerospace Corporation's proprietary software "HyperSeal". This software has been designed to perform the following:
    a) Conversion of digital counts to radiance values using the in-flight calibration measurements made with the two blackbodies mounted in the same well in the aircraft belly as the sensor. These blackbodies swing into the sensor's FOV once before the target line begins and once more after the target line has been completed. From the blackbody calibration, a post-processing technique will yield the SEBASS's LWIR/MWIR NESR curves. This NESR curve will be different at each altitude, since the sensor software must be set to a different co-add value.

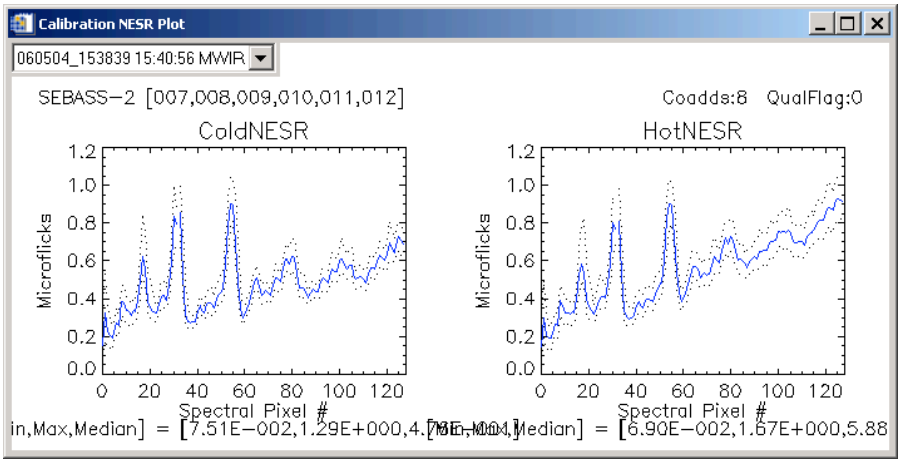

Fig. 6: NESR plots for cold (15 degrees C) and hot (40 degrees C) calibration blackbodies at eight co-adds for the 6000 ft AGL flight line.

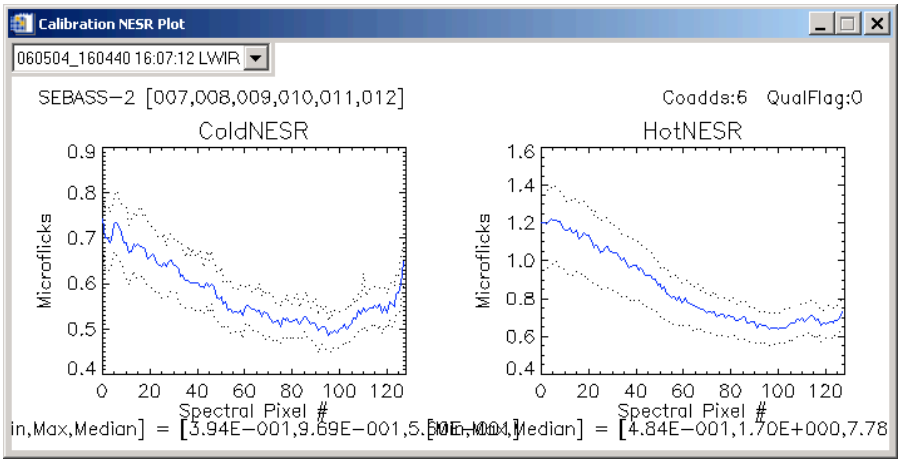

Fig. 7: NESR plots for cold (15 degrees C) and hot (40 degrees C) calibration blackbodies at six co-adds for the 4500 ft AGL flight line.

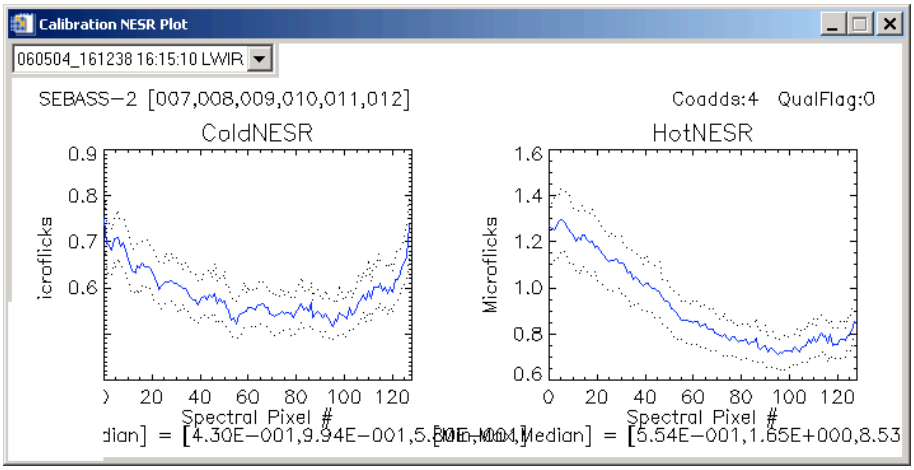

Fig. 8: NESR plots for cold (15 degrees C) and hot (40 degrees C) calibration blackbodies at four co-adds for the 3000 ft AGL flight line.

b) Atmospheric calibration of the radiance data is performed using another of The Aerospace Corporation's proprietary pieces of software called the In-Scene Atmospheric Compensation (ISAC) routine[6,7]. ISAC makes the assumption that for a given wavelength there are measurements within the scene of a target with an emissivity of one. High emissivity materials are usually vegetation and water, which is why most flight lines are setup so that there is at least water and/or vegetation within the target scene. The material does not have to be a blackbody at all wavelengths. MODTRAN is not utilized by ISAC, since ISAC itself compensates for atmospheric transmission and upwelling radiance values. ISAC does not however, compensate for the downwelled radiance factor. This lack of compensation will show up later in the analysis section when a target has a high reflectance in the LWIR.

i. ISAC is applied by first calculating the wavelength that has the highest brightness temperature. This is then set as the reference wavelength. For each wavelength, a scatterplot is created using the reference radiance scaled to the blackbody radiance at the given wavelength as the x-values, and y-values are the measured radiance at the given wavelength. A line is then fit to the highest points on the scatterplot. Then the atmospheric compensation can be applied to the data using the linear regression of the curve fit[6,7].

$$radiance_{comp} = \frac{radiance_{uncomp} - offset}{slope} \qquad (2)$$

c) The compensated radiance is then converted to apparent emissivity values by a ratio of the measured radiance to the calculated blackbody radiance at a reference temperature. Once the data is in this format, it can now be compared to other hyperspectral cubes in this format, and also library emissivity spectra values.

2) SEBASS apparent emissivity cubes were then loaded into ENVI to map out and plot individual pixel spectral values for desired targets.

a) Overplots were made for each altitude (3000, 4500, 6000 ft AGL) for each individual target so that the correlations between different altitudes could be easily observed (Each target will have four plots, one for each altitude, and one laboratory spectra). Lower altitudes will have more "pure" pixels, meaning that the higher GSD cubes will have a larger chance of having mixed pixels, especially at the edges of the targets.

b) Spectral math will be performed on each target to assess differences in band depth and transmission factors. Spectral subtraction and spectral ratios are two spectral math techniques that will be employed.

5.0 Results and Discussion

A sample SEBASS hyperspectral cube is displayed in Figure 9. One band is selected and displayed in grayscale to provide spatial information about target location. The cube is one hundred and twenty eight pixels wide and two thousand two hundred lines long. As the altitude is decreased and airspeed remains constant, flight lines must consist of more lines and lower 'co-add' value, since the ground is now moving past the sensor window at a faster rate. The way this strip is orientated, the direction of travel of the aircraft would be horizontally (left to right) across the page.

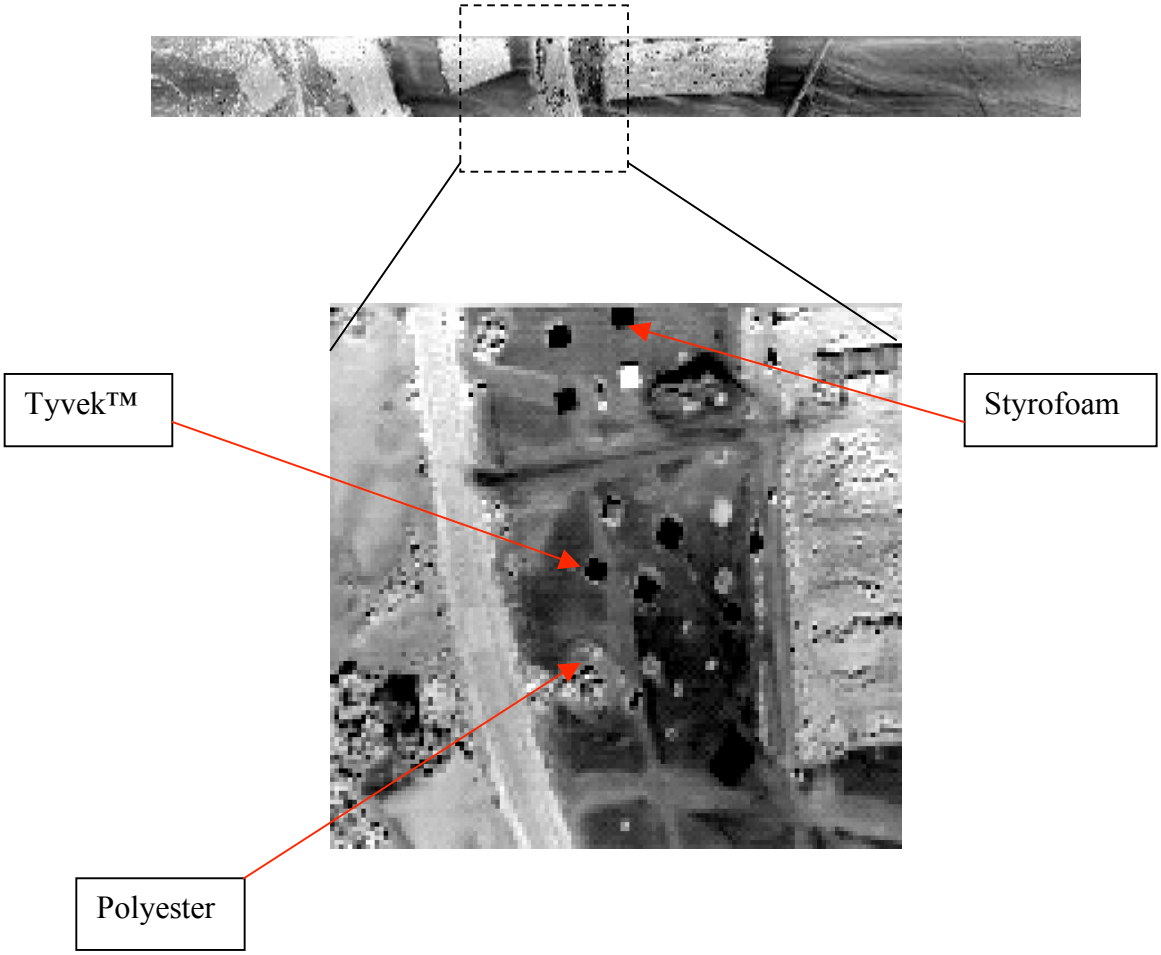

Fig. 9: Actual SEBASS Strip image (top) and zoom image (bottom) of the target area at 3000 ft AGL. Targets are located in the center of the strip.

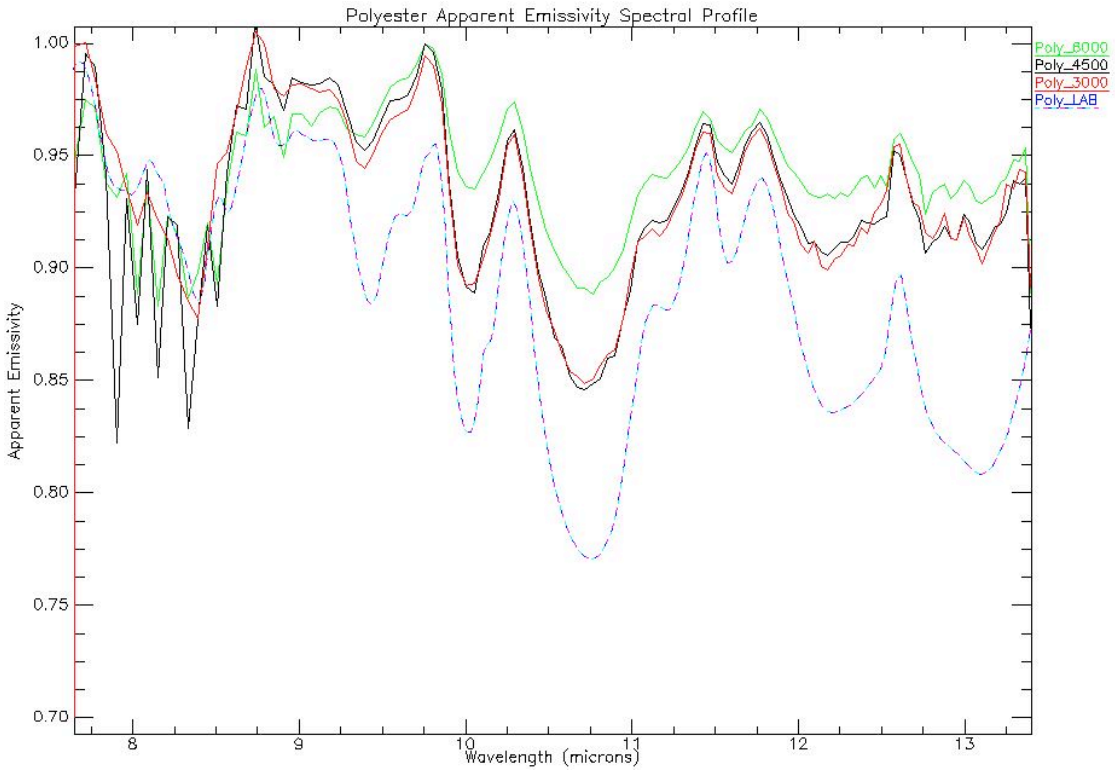

Fig. 10: Spectrum plots of polyester target pixels.
Lab reference spectrum is plotted as a dashed blue line.

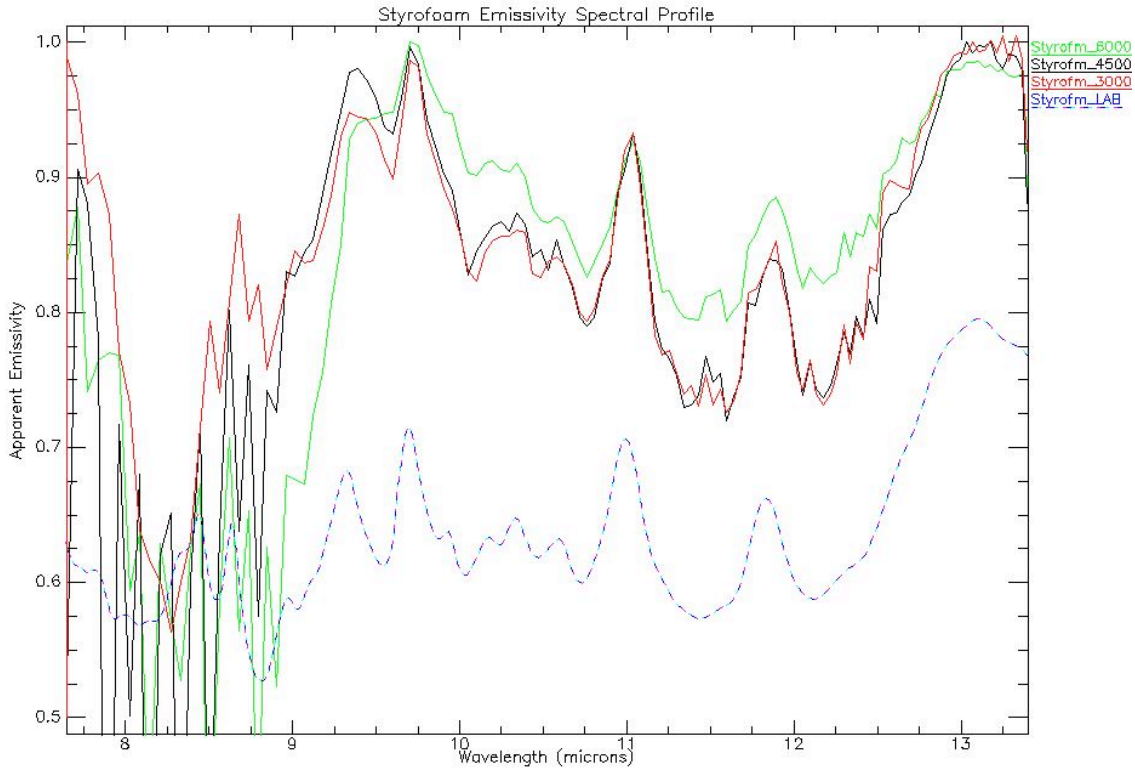

Fig. 11: Spectrum plots of Styrofoam target pixels.
Lab reference spectrum is plotted as a dashed blue line.

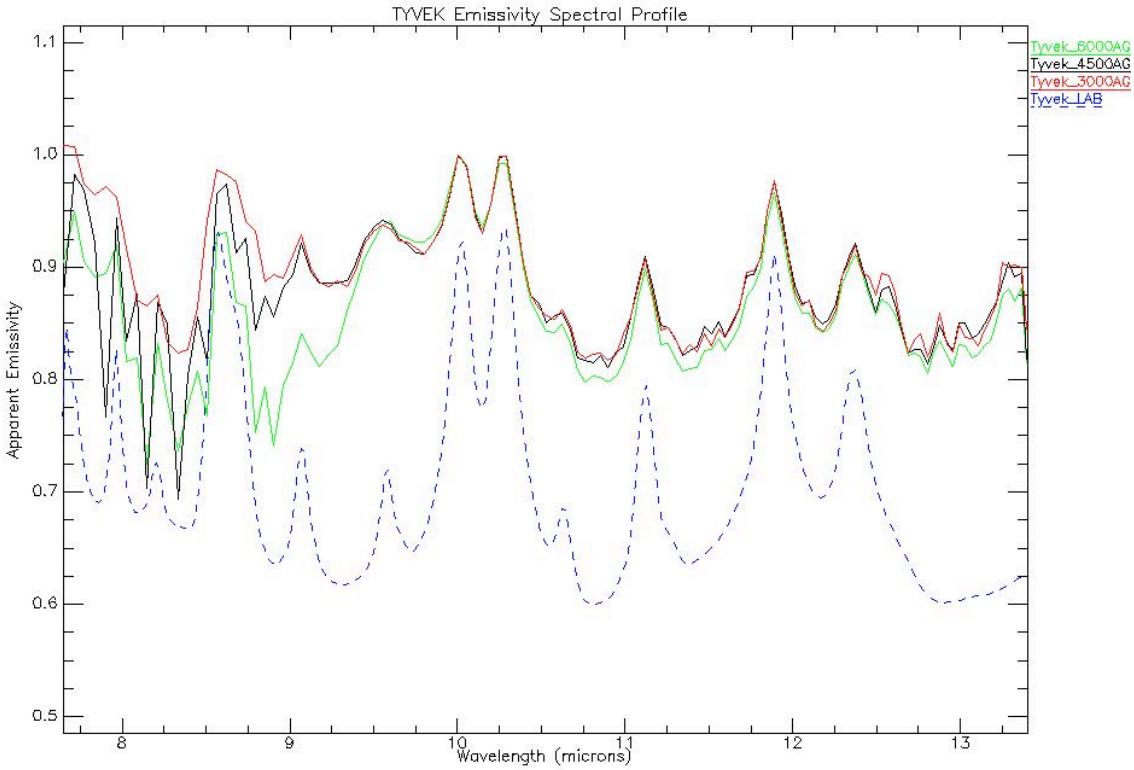

Fig. 12: Spectrum plots of a Tyvek™ target pixels.
Lab reference spectrum is plotted as a dashed blue line. One of the smallest peaks is at 10.6 microns and it is easily discernable at every altitude.

Upon examination of each of the three target apparent emissivity plots (Figures 10-12), it can be immediately observed that the apparent emissivity curves at each altitude are extremely comparable to the measured laboratory spectra. As stated before, the targets were chosen for their features within the LWIR region, and the multiple apparent emissivity peaks/troughs show up vividly in each plot. Towards the shorter end of the spectrum, noise enters the plots in the form of possible reflected downwelling, which could be a result from errors in the atmospheric correction technique. This is very apparent in Figure, 11, the plots of the Styrofoam. Towards the longer end of the region, the influence of carbon dioxide within the atmosphere begins to have an effect on the emissivity curves. For the most part however, these sample plots in the above figures display extraordinary amount of accuracy and spectral fitment to the recorded laboratory curves.

	Apparent Emissivity Peak Locations for Polyester (microns)													
Altitude(ft AGL)	7.68	8.1	8.51	8.76	8.97	9.16	9.6	9.8	10.29	11.12	11.45	11.78	12.61	13.6
3000	x	x	o	x	x	x	x	x	x	x	x	x	x	x
4500	x	x	o	x	x	x	x	x	x	x	x	x	x	x
6000	x	x	o	x	x	x	x	x	x	x	x	x	x	x

	Apparent Emissivity Peak Locations for Styrofoam (microns)											
Altitude(ft AGL)	8.44	8.64	8.97	9.32	9.65	9.93	10.17	10.33	10.59	10.99	11.85	13.09
3000	*	*	x	x	x	o	o	x	x	x	x	x
4500	*	*	x	x	x	o	x	x	x	x	x	x
6000	*	*	x	o	x	o	x	x	x	x	x	x

	Apparent Emissivity Peak Locations for Tyvek(TM) (microns)												
Altitude(ft AGL)	7.53	7.67	7.96	8.2	8.57	9.06	9.58	10.03	10.27	10.65	11.13	11.89	12.38
3000	x	x	x	x	x	x	x	x	x	x	x	x	x
4500	x	x	x	x	x	x	x	x	x	x	x	x	x
6000	x	x	x	x	x	x	x	x	x	x	x	x	x

Fig. 13 & 14 & 15: Charts illustrating whether or not the sample apparent emissivity data sets possess the same peaks as the laboratory apparent emissivity peaks. An 'x' means the sample data possesses a peak at the reference spectra peak location. An 'o' means there was no discernable peak in the sample data. '*' Denotes possible reflected downwelled radiance is drowning out any emissivity peaks that may be observed.

It should be noted that there exist a few bad pixels within the long-wave focal plane array. Most of these pixels are scattered in the shorter wavelengths of the long-wave FPA. Channel zero is completely dead so it is disregarded in all of the previous analysis. The 'HyperSeal' program accounts for these dead pixels by performing an interpolation across each dead pixel. However, there is still plenty of each target's features present within the middle of the spectral range and without a doubt they provide a definitive answer to the question of whether apparent emissivity values are altitude dependent. Going one step further, band math can be performed on the target spectra to observe any relationship between apparent emissivities at two different altitudes.

Once the target pixel had been selected, ENVI's band math function make the analysis elementary. Each one of the three altitudes was operated on with the other two (6000& 4500, 6000& 3000, and 4500& 3000) with the results shown below. Using spectral subtraction will illustrate how band depth varies with altitude. Using a spectral ratio technique will enhance the differences between two spectra. Dividing one spectrum by another will produce a plot that illustrates relative spectral intensities. Each method described will be helpful in analyzing just how the apparent emissivities at each altitude compare to one another, which will hopefully provide further support for the hypothesis that pixel size does not influence recorded apparent emissivity within the LWIR region.

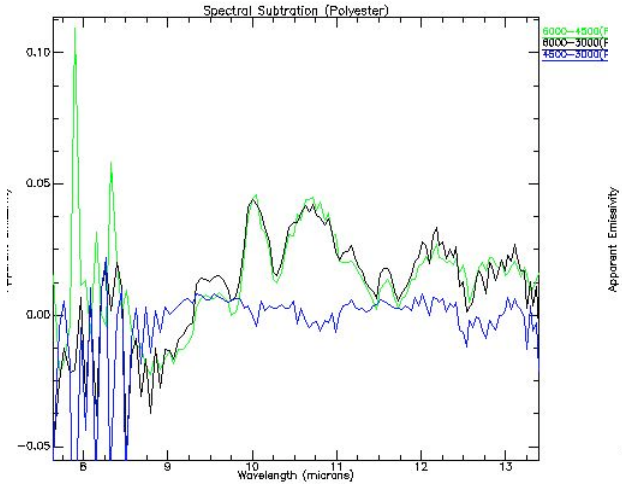

Fig. 16: Spectral subtraction comparison of the multiple altitude lines for the polyester target.

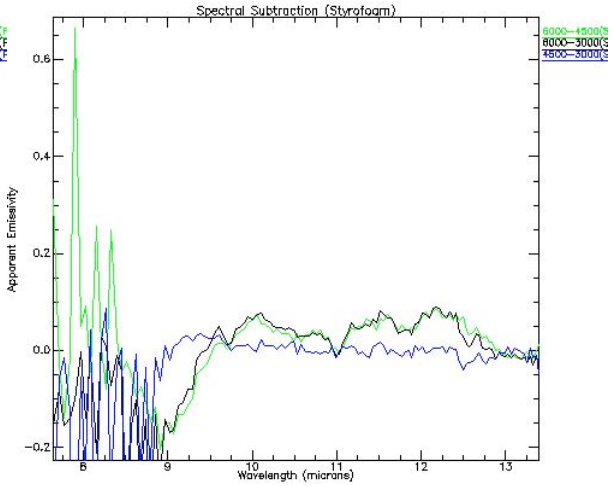

Fig. 17: Spectral subtraction comparison of the multiple altitude lines for the Styrofoam target.

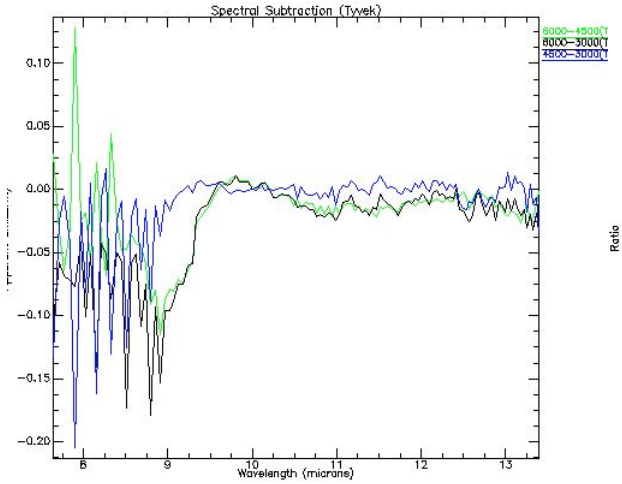

Fig. 18: Spectral subtraction comparison of the multiple altitude lines for the Tyvek™ target.

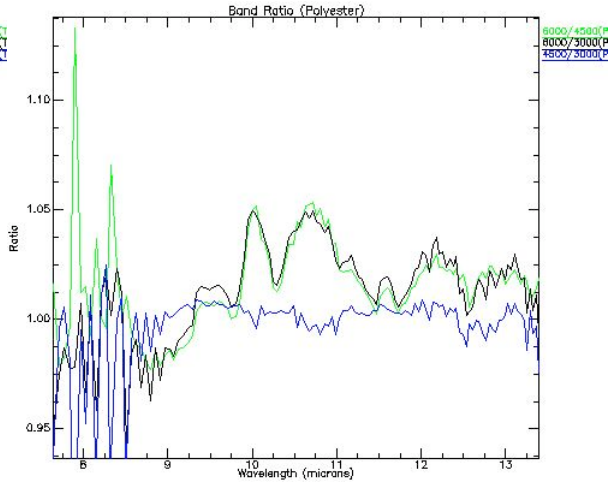

Fig. 19: Spectral ratio comparison of the multiple altitude lines for the polyester target.

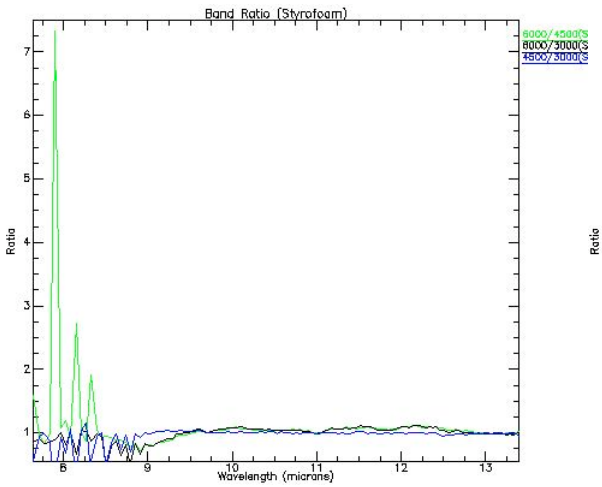

Fig. 20: Spectral ratio comparison of the multiple altitude lines for the Styrofoam target. (Note the three maxima At the shorter wavelengths due to the target reflecting downwelled radiance)

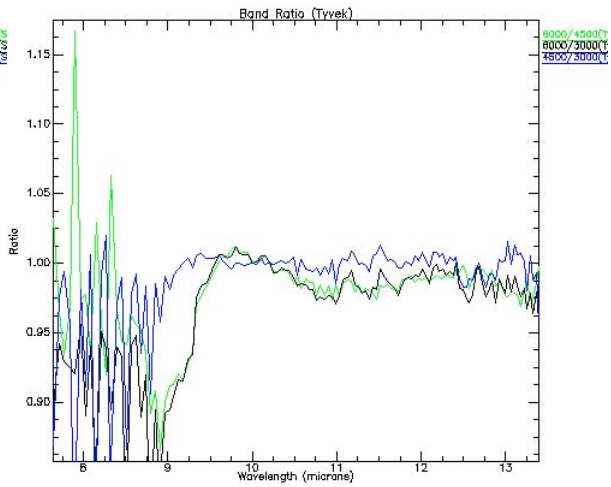

Fig. 21: Spectral ratio comparison of the multiple altitude lines for the Tyvek™ target.

The spectral subtraction results illustrated how similar each altitudes spectral plot is, with exception to the shorter wavelengths. From nine to thirteen microns the absolute average spectral difference for each plot was approximately between .01 and .08, at most an 8% difference in spectral reflectance. Working within the same region when dealing with the results from the spectral ratio, the same can be said, that the absolute average spectral ratio stays between +/- 5% of 1.00 (1.00 meaning the two spectra are identical).

6.0 Conclusion

Even though the results of the spectral subtraction and spectral ratio techniques exhibit some anomalies, particularly with the Styrofoam target, I believe that the purpose of this paper, which was to prove that pixel size does not impact observed apparent emissivity values of targets with LWIR characteristics, when all other variables remain constant, has been validated. Going back to Figures 13-15, we see that for polyester, 13 out of 14 band peaks were detected at *every* altitude. For the Styrofoam target, 8 out of 12 band peaks were detected at the 3000 and 4500 ft flight lines, while 7 out of 12 were detected at the 6000 ft altitude. But the best test case was undoubtedly the Tyvek™, in which every single band was detected at each altitude. Whether datasets are processed via human or machine means, the methods will be different, human psychophysics or machine byte processing, but the results will be that these signatures will be found each and every time.

It might be suggested that the altitudes chosen for this experiment are not applicable or indicative of space-based sensor platforms. I disagree, it has been demonstrated that with adequate atmospheric correction, even the simplest emissivity conversion has shown accurate spectral results across the ranges of altitudes for each target selected. An attempt to repeat this experiment at higher altitudes and thus even smaller pixels would run into the problem that the targets would have to be large enough so that at least one pixel would be

100% target. This would have meant uniform targets would have to be constructed larger than five meters square, which then would have additional logistical difficulties. I feel that the altitudes selected for this experiment represent a good trade-off of pixel and target size.

7.0 Future Plans

7.1 SpectIR VNIR/SWIR data

This data set is particularly rich in targets with a broad range of spectral features, both in the emissive and reflective regions. Once the SpectIR data is delivered, the same analysis could be performed on the VNIR/SWIR datasets, which would be another informative example. The results from that analysis would either refute or further support the conclusions made in this paper.

7.2 SEBASS MWIR data

Likewise for SEBASS's mid-wave IR data. A few targets that have long-wave features also exhibit some mid-wave characteristics, such as Styrofoam and polyester. Further analysis on the Styrofoam target to eliminate the reflected downwelling vector would 'smooth' out the spectral ratio curve and perhaps allow some of the shorter wavelength features to be observed.

7.3 SEBASS Lab measurements

Mentioned earlier in the paper, was the ability of SEBASS to be mounted on a rack in a laboratory type atmosphere with specialized optics that allows samples to be placed directly under the sensor window (~10cm). Small samples of each target were taken in order to analyze once again but using SEBASS in its rack-type configuration. This allows for the complete negation of any atmospheric effects, transmission, upwelled/downwelled radiance, and will provide the most accurate emissivity results. I would like to take each of the three targets talked about in the paper today and measure them in this fashion.

8.0 References

1. L.E. Kirkland, K.C. Herr, E.R. Keim, P.M Adams, J.W. Salisbury, J.A. Hackwell, A Treiman, "First use of an airborne thermal infrared hyperspectral scanner for compositional mapping", *Remote Sensing of Environment*, Sep. 2001.
2. N.G. Raqueno, L.E. Smith, D.W. Messinger, C. Salvaggio, R.V. Raqueno, J.R.Schott, "Megacollect 2004: hyperspectral collection experiment of terrestrial targets and backgrounds of the RIT Megascene and surrounding area", *SPIE,* Vol. 5806, 2005.
3. T. Bowers, "Comparison of the effects of variable spatial resolution on hyperspectral-based geologic mapping", Algorithms and Technologies for Multispectral and Ultraspectral Imagery IX, *Proceedings of SPIE*, Vol. 5093, 2003.
4. F.A. Kruse, "The effects of spatial resolution, spectral resolution, and SNR on geologic mapping using hyperspectral data, Northern Grapevine Mountains, Nevada", *Proceedings of the 9th JPL Airborne Earth Science Workshop*, JPL Pub 00-18, 2000.
5. J.A Hackwell, D.W. Warren, R.P. Bongiovi, S.J. Hansel, T.L. Hayhurst, D.J. Mabry, M.G. Sivjee, J.W. Skinner, "LWIR/MWIR imaging hyperspectral sensor for airborne and ground-based remote sensing," *SPIE,* Vol. 2819, 1996.
6. B.R. Johnson, "Inscene atmospheric compensation: application to the SEBASS data collected at the ARM Site, Part I." *Aerospace Report ATR-99(8407), Part I.* 1998

7. S.J., Young, “Inscene atmospheric compensation: application to the SEBASS data collected at the ARM Site, Part II.” *Aerospace Report ATR-99(8407), Part II*. 1998
8. L.E. Kirkland, K.C. Herr, P.M. Adams, J. McAfee, J. W. Salisbury, “Thermal infrared hyperspectral imaging from vehicle-carried instrumentation”, *SPIE*, Vol. 4816, 2002.
9. J.R. Schott, *Remote Sensing: The Image Chain Approach*, (Oxford Press, New York, 1997), pp 114-119.
10. Philipona, R., E.G. Dutton, T. Stoffel, J. Michalsky, I. Reda, A. Stifter, P. Wendling, N. Wood, S.A. Clough, E.J. Mlawer, G.P. Anderson, H.E. Revercomb, T.S. Shippert, “Atmospheric longwave irradiance uncertainty: Pyrgeometers compared to an absolute sky-scanning radiometer, atmospheric emitted radiance interferometer and radiative transfer model calculations”, *J. Geophys*. Res., 106, 28129-28142, 2001.
11. Anderson, G. P., A. Berk, P. K. Acharya, M. W. Matthew, L. S. Bernstein, J. H. Chetwynd, H. Dothe, S. M. Adler-Golden, A. J. Ratkowski, G. W. Felde, J. A. Gardner, M. L. Hoke, S. C. Richtsmeier, B. Pukall, J. Mello and L. S. Jeong, “MODTRAN4: Radiative transfer modeling for remote sensing, in algorithms for multispectral, hyperspectral, and ultraspectral imagery VI”, Sylvia S. Chen, Michael R. Descour, Editors, *Proceedings of SPIE* Vol. 4049, pg. 176-183, 2000.
12. L.E. Kirkland, K.C. Herr, J.W. Salisbury, “Thermal infrared spectral band detection limits for unidentified surface materials”, *Applied Optics*, May 2001.
13. B. Hapke, *Theory of Reflectance and Emittance Spectroscopy*, (Cambridge UP,1993).
14. C.S. Williams, O.A. Becklund, *Optics: A Short Course for Engineers*, Krieger, Malabar, pp. 58-63.
15. C. Salvaggio, L.E. Smith, E.J. Antoine, “Spectral signature databases and their application/misapplication to modeling and exploitation of multispectral/hyperspectral data”, *SPIE,* Vol. 5806, 2005.
16. S.M. Schweizer, J.M.F. Moura, “Efficient detection in hyperspectral imagery”, *IEEE*, Vol.4, No.4, April 2001.